

## Purdue University Purdue e-Pubs

---

Department of Electrical and Computer  
Engineering Faculty Publications

Department of Electrical and Computer  
Engineering

---

2016

# Thermodynamic efficiency limits of classical and bifacial multi-junction tandem solar cells: An analytical approach

Muhammad A. Alam  
*Purdue University*, [alam@purdue.edu](mailto:alam@purdue.edu)

Mohammad Ryyan Khan  
*Purdue University*, [khan23@purdue.edu](mailto:khan23@purdue.edu)

Follow this and additional works at: <http://docs.lib.purdue.edu/ecepubs>

 Part of the [Electrical and Computer Engineering Commons](#)

---

Alam, Muhammad A. and Khan, Mohammad Ryyan, "Thermodynamic efficiency limits of classical and bifacial multi-junction tandem solar cells: An analytical approach" (2016). *Department of Electrical and Computer Engineering Faculty Publications*. Paper 69.  
<http://dx.doi.org/10.1063/1.4966137>

This document has been made available through Purdue e-Pubs, a service of the Purdue University Libraries. Please contact [epubs@purdue.edu](mailto:epubs@purdue.edu) for additional information.

## Thermodynamic efficiency limits of classical and bifacial multi-junction tandem solar cells: An analytical approach

Muhammad Ashraful Alam and M. Ryyan Khan

Citation: [Applied Physics Letters](#) **109**, 173504 (2016); doi: 10.1063/1.4966137

View online: <http://dx.doi.org/10.1063/1.4966137>

View Table of Contents: <http://scitation.aip.org/content/aip/journal/apl/109/17?ver=pdfcov>

Published by the [AIP Publishing](#)

---

### Articles you may be interested in

[Theoretical efficiency limit for a two-terminal multi-junction “step-cell” using detailed balance method](#)

[J. Appl. Phys.](#) **119**, 073104 (2016); 10.1063/1.4942223

[Thermodynamic limit of bifacial double-junction tandem solar cells](#)

[Appl. Phys. Lett.](#) **107**, 223502 (2015); 10.1063/1.4936341

[Wafer Processing Aspects of High Efficiency Multi-junction Solar Cells](#)

[AIP Conf. Proc.](#) **1407**, 38 (2011); 10.1063/1.3658290

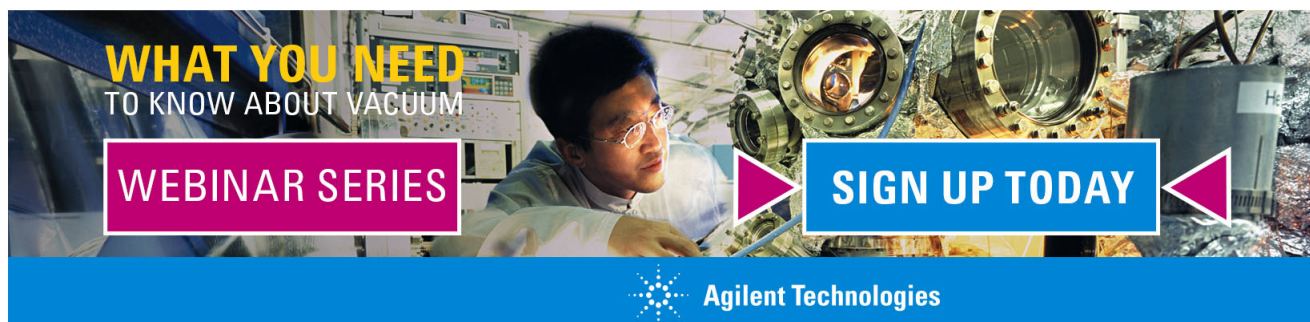
[Detailed balance limit of the efficiency of multilevel intermediate band solar cells](#)

[Appl. Phys. Lett.](#) **98**, 171108 (2011); 10.1063/1.3583587

[Statistical thermodynamic foundation for photovoltaic and photothermal conversion. IV. Solar cells with larger-than-unity quantum efficiency revisited](#)

[J. Appl. Phys.](#) **89**, 2482 (2001); 10.1063/1.1338522


---

A promotional banner for Agilent Technologies. It features a background image of a person in a lab coat working with a piece of equipment. The text 'WHAT YOU NEED TO KNOW ABOUT VACUUM' is in yellow and white. Below it, a pink box says 'WEBINAR SERIES' and a blue box says 'SIGN UP TODAY'. The Agilent logo and name are at the bottom.

**WHAT YOU NEED**  
TO KNOW ABOUT VACUUM

**WEBINAR SERIES**

**SIGN UP TODAY**

 **Agilent Technologies**

# Thermodynamic efficiency limits of classical and bifacial multi-junction tandem solar cells: An analytical approach

Muhammad Ashraful Alam<sup>a)</sup> and M. Ryyan Khan

School of Electrical and Computer Engineering, Purdue University, West Lafayette, Indiana 47907, USA

(Received 24 June 2016; accepted 11 October 2016; published online 25 October 2016)

Bifacial tandem cells promise to reduce three fundamental losses (i.e., above-bandgap, below bandgap, and the uncollected light between panels) inherent in classical single junction photovoltaic (PV) systems. The successive filtering of light through the bandgap cascade and the requirement of current continuity make optimization of tandem cells difficult and accessible only to numerical solution through computer modeling. The challenge is even more complicated for bifacial design. In this paper, we use an elegantly simple analytical approach to show that the essential physics of optimization is intuitively obvious, and deeply insightful results can be obtained with a few lines of algebra. This powerful approach reproduces, as special cases, all of the known results of conventional and bifacial tandem cells and highlights the asymptotic efficiency gain of these technologies. *Published by AIP Publishing.* [<http://dx.doi.org/10.1063/1.4966137>]

The optimum single junction (SJ) solar cell fails to convert 2/3 of the incident sunlight into useful energy.<sup>1,2</sup> In fact, these unconverted sub-bandgap (sub-BG) and above-bandgap (above-BG) photons further degrade the performance and reliability through self-heating.<sup>3,4</sup> Moreover, the panels in a solar farm must be spatially separated to avoid shadowing; as a result, ~50% of the photons are wasted in the space in between (space-loss).<sup>5</sup> With this “space-loss” accounted for, ~83% of the sunlight incident on a solar farm will never be converted to electricity.

A bifacial multi-junction tandem (B-MJT) cell promises to stem these three fundamental losses as follows: photons of various energies are converted by the sequence of absorbers with decreasing bandgaps so that “sub-BG” and “above-BG” losses are reduced in half.<sup>6</sup> In addition, bifacial cells partially recover (~30% in practice) the space-loss by converting the albedo light,<sup>7–10</sup> see Fig. 1(a). Therefore, in principle, a B-MJT solar farm may be 250% more efficient than a SJ solar farm.

Since the 1960s, many groups have analyzed the physics and optimized the design of MJTs with a finite number of cells.<sup>6,11–14</sup> Although the concept of bifacial cells<sup>15–17</sup> is not new, their high efficiency and reduced temperature sensitivity have sparked recent commercial interest. The thermodynamics and the optimization of two-junction bifacial cells have been reported recently.<sup>9,10</sup> The results show that the optimization is nontrivial: In a classical MJT, the need for current-matching dictates a sequential decrease in bandgap from the top to the bottom. In a B-MJT, the bottom cell is illuminated by albedo light; therefore, we need not maintain the bandgap sequence; a partial inversion of bandgaps is possible and desirable.

Even in the idealized thermodynamic limit, however, many questions remain unanswered: What is the optimum bandgap sequence of a B-MJT and how does it compare to a classical MJT? How would the configuration change when the solar farm is installed on a grass vs. a concrete surface?

At what point is the marginal gain in power output offset by the cost of the additional junction?

A numerical simulation can answer these questions, but the essential physics is sometimes lost in the fog of numerical modeling. Instead, we use a simple approximation for bandgap-dependent photocurrent, within a chained-form system,<sup>18</sup> to show that the choice of bandgap in classical vs. B-MJT is described by an elegantly simple formulation. We assume a 2-terminal tandem with all of the subcells connected electrically in series. The optimum efficiency predicted by the model matches the numerical results within ~2%. Away from the optimum BG, the luminescence coupling<sup>19,20</sup> is essential and numerical modeling cannot be

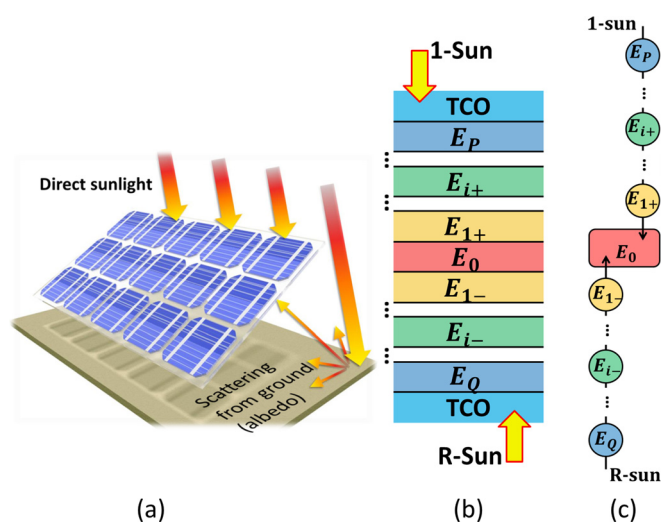


FIG. 1. (a) A bifacial panel collects both the direct sunlight and the light scattered from ground (albedo reflectance,  $R$ ). Reproduced with permission from Appl. Phys. Lett. **106**, 243902 (2015). Copyright 2015 AIP Publishing. (b) A bifacial multi-junction tandem (B-MJT) is shown. The cell receives 1-Sun and  $R$ -Sun illuminations from the top and the bottom, respectively. (c) The B-MJT shown in (b) can be viewed as a bubble chain. The cells above  $E_0$  absorb direct sunlight from the top, while those below  $E_0$  absorb albedo light from the bottom. The absorber with the smallest bandgap ( $E_0$ ) absorbs light from both sides.

<sup>a)</sup>Electronic mail: alam@purdue.edu

avoided. Even in those cases, the results of the calculation provide excellent initial guesses regarding the potential of the bifacial cell technology.

Fig. 1(b) represents the typical configuration of a bifacial cell. Conceptually, a B-MJT may be represented, as in Fig. 1(c), by a chain of bubbles (each representing a material with bandgap,  $E_g$ , and short-circuit current,  $J_{SC}(E_g)$ ), illuminated by 1-sun on the top and  $R$ -sun at the bottom. The cell with the smallest bandgap ( $E_0 \equiv E_{g,min}$ ) is located at  $\{0\}$ , which need not be at the bottom. The segment of the chain illuminated by the direct incident light from the top is marked  $\{i+\}$ , with the top cell at  $\{P\}$ . Similarly, the cells illuminated by the albedo light from the bottom are marked  $\{i-\}$ , with the bottom cell at  $\{Q\}$ . Thus, the total number of cells is  $N \equiv P + Q + 1$ .

Assuming complete absorption above the bandgap, the current in the individual bubbles is related to the short circuit current  $J_{SC}(E_g)$  of isolated absorbers as follows:

$$J_{\{i\pm\}} = J_{SC,i\pm} - J_{SC,(i+1)\pm}, \text{ except that,} \quad (1)$$

$$J_P = J_{SC,P} \quad (\text{top cell}), \quad (2)$$

$$J_Q = R J_{SC,Q} \quad (\text{bottom cell}). \quad (3)$$

Since the current through the series connected cells must be identical, the equations above are numerically equal.

Despite the complexity of the AM1.5G spectrum, the short-circuit current,  $J_{SC}(E_g)$ , scales almost linearly within the bandgap range ( $0.5 \text{ eV} < E_g < 1.9 \text{ eV}$ ). In general, we can always map  $E_g$  to  $X_g$ , so that

$$J_{SC}(X_g) = J_{SUN}(1 - \beta X_g), \quad (4)$$

where  $\beta$  is a constant, and  $J_{SUN}$  depends on intensity,  $I$ . Unlike the ‘‘actual bandgap’’  $E_g$ , the ‘‘mapped bandgap’’  $X_g$  is always linear with  $J_{SC}$ . This mapping greatly simplifies the analysis for MJTs and B-MJTs. Once  $X_g$  is solved explicitly (discussed later), it can be trivially mapped back to  $E_g$ , as shown in Fig. S1 of the [supplementary material](#).

Inserting Eq. (4) into Eqs. (1)–(3) and dictating that the current must be continuous through the tandem cells, we find that the bandgap optimization problem can be solved as follows:

$$[X] = [M]^{-1}[Z], \quad (5)$$

where  $[X] = [X_P, \dots, X_{i+}, \dots, X_{j-}, \dots, X_Q]$  is the bandgap vector of size  $N - 1$  (excluding  $X_0$ ), and the residual vector,  $[Z]$ , of the same size is given by

$$[Z] = \begin{cases} -[1, 0, 0, \dots, \beta(1+R)X_0, \beta(1+R)X_0, \\ \dots, 0, 0, R]; P, Q > 0 \\ -[1, 0, 0, \dots, \beta(1+R)X_0 - R]; P > 0, Q = 0 \\ -[1 + \beta(1+R)X_0 - R]; P = 0, Q = 0 \end{cases} \quad (6)$$

and  $[M] \equiv \begin{bmatrix} \beta \nabla_P^2 & B_R \\ B & R\beta \nabla_Q^2 \end{bmatrix}$ , where  $R$  is the effective albedo reflectance, and

$$[\nabla^2] \equiv \begin{bmatrix} -2 & 1 & \dots & \dots \\ 1 & -2 & 1 & \dots \\ \dots & \dots & \ddots & \dots \\ \dots & \dots & 1 & -2 \end{bmatrix}, \quad [B] \equiv \begin{bmatrix} 0 & \dots & -\beta \\ \vdots & \ddots & \vdots \\ 0 & \dots & 0 \end{bmatrix},$$

$$[B_R] \equiv \begin{bmatrix} 0 & \dots & 0 \\ \vdots & \ddots & \vdots \\ -\beta R & \dots & 0 \end{bmatrix}.$$

Note that  $[\nabla_P^2]$  is a  $P \times P$  matrix. Once Eq. (5) is solved for  $[X]$ , the actual bandgap set  $[E]$  can be obtained by inverse mapping as discussed earlier (also see Fig. S1).

Once the vector  $[E]$  is specified, the full  $J - V$  characteristics

$$J(V) = J_{ph} - J_{dark}(V), \quad (7)$$

can be determined as follows (see [supplementary material](#) for details). The photocurrent,  $J_{ph}$ , of the tandem device is proportional to the number of solar photons absorbed in a subcell, with this optical process being independent of bias  $V$ . The photocurrents of the subcells are matched, and therefore can be replaced by a single source, evaluated  $J_{ph} = J_P$ , for example. The dark current is

$$J_{dark}(V) \equiv J_{D,i} = A_i(E_i)(e^{qV_i/k_B T_D} - 1). \quad (8)$$

Here,  $A_i(E_g) = q\Omega_{D,i} \gamma(E_g, T) e^{-E_g/k_B T_D}$  and  $\gamma(E_g, T) \equiv (2k_B T/c^2 h^3)(E_g^2 + 2k_B T^2 E_g + 2k_B^2 T^2)$  (see Ref. 2). We define  $A_i(E_i)$  such that it accounts for photon recycling within each subcell. Here,  $T_D$  is the device temperature, and  $\Omega_{D,i}$  is the emission angle from each subcell. If the luminescent coupling among the subcells is negligible,  $\Omega_{D,i} = 4\pi$  (or  $2\pi$ ) for the bifacial (or conventional) device.

Using Eq. (8), we can write

$$V = \sum_N V_i = \sum_N \frac{k_B T_D}{q} \ln \left( \frac{J_{dark}}{A_i} + 1 \right) = \frac{k_B T_D}{q} \ln \left( \frac{J_{dark}^N}{\prod A_i} \right),$$

$$\therefore J_{dark}(V) \approx q\Omega_D^* \{\gamma_i\} e^{-\langle E_g \rangle / k_B T_D} e^{(qV/Nk_B T_D)}. \quad (9)$$

Here,  $\langle E_g \rangle$  is the arithmetic mean of the bandgap set  $[E]$ .  $\Omega_D^*$  and  $\{\gamma_i\}$  are the geometric means of  $\Omega_{D,i}$  and  $\gamma(E_i, T_D)$ , respectively. In this remarkable result, Eq. (9) suggests that the terminal response of the complex B-MJT can be represented by a string of identical cells repeated  $N$ -times, making the vast literature on the SJ physics available to MJT analysis.

To summarize, once  $X_0$ ,  $N$ ,  $Q$  (or,  $P$ ), and  $R$  are specified, Eq. (5) is solved to obtain the bandgap-set  $[X]$ . The values  $[X]$  do not represent the final bandgaps and are required to be mapped into the ‘‘actual bandgaps’’  $[E]$ . Then, Eqs. (1)–(3), (7), and (9) can be used to construct the  $J - V$  characteristics and the efficiency,  $\eta_T^*(E_0, N, Q, R)$ , of the cells. This is how we calculate the contour plot shown in Fig. 2(a), for the specific case of ( $Q = 0$ , and  $R = 0$ ), to be discussed below. To calculate the optimum output power,  $P_{max} \equiv J(V_{opt})V_{opt}$ , we must first calculate the voltage  $V_{opt}$  at the maximum power

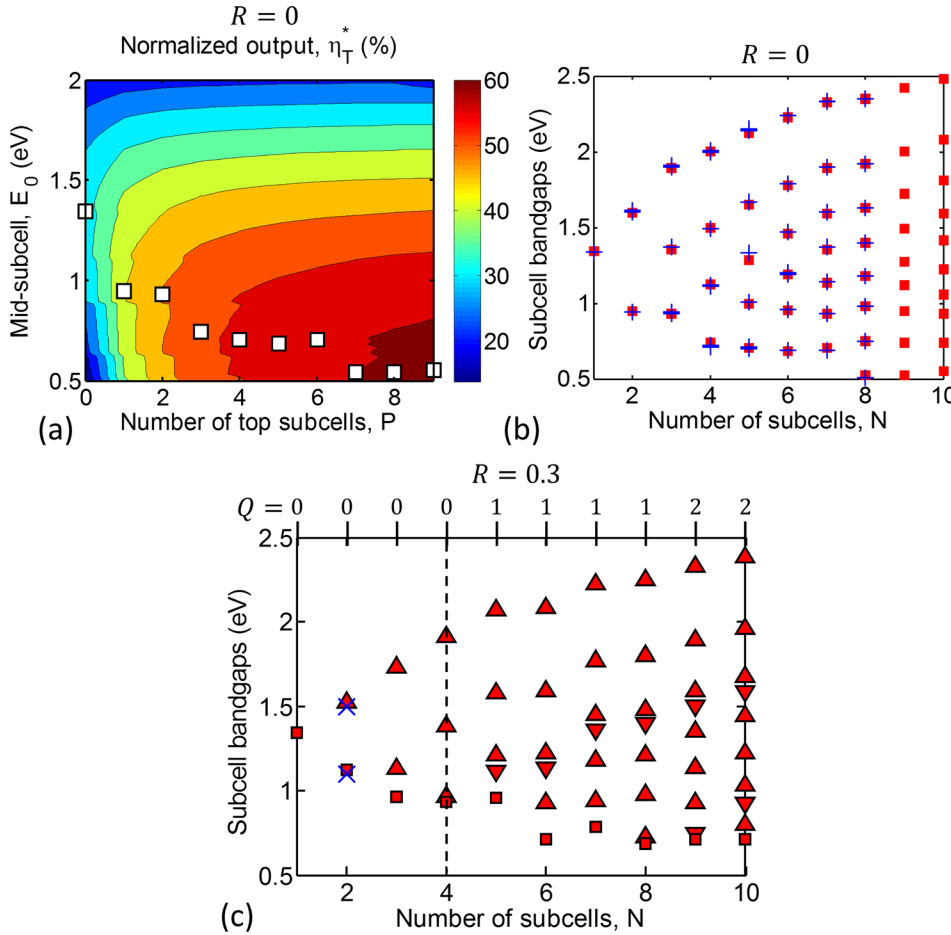


FIG. 2. (a) The normalized B-MJT output  $\eta_T^*$  is for  $Q=0$  found as functions of  $P$  and  $E_0$  at  $R=0$ . The optimum  $E_0$  is marked as white squares. Note that,  $N=P+1$  as we have set  $Q=0$  in this case. (b) shows the corresponding optimum B-MJT bandgaps (red-filled squares). Results are compared to theoretical predictions in the literature for the conventional tandem (+).<sup>13,14</sup> (c) The optimum B-MJT bandgaps for  $R=0.3$  are shown. The squares ( $\square$ ) show the  $E_0$ -values. The  $\Delta$  and  $\nabla$  markers represent the bandgaps for the front  $\{i+\}$  and back  $\{j-\}$  subcells, respectively. The results are compared to the bifacial tandem ( $\times$ ) literature.<sup>10</sup>

output. To do so, we solve Eq. (9) (by using the technique in Ref. 2) to obtain

$$\frac{qV_{opt}}{N} \approx \langle E_g \rangle \left( 1 - \frac{T_D}{\langle E_g \rangle} \frac{E_{g,P}}{T_S} \right) - k_B T_D \ln \left( \frac{\Omega_D^*}{\Omega_S} \right). \quad (10)$$

Here,  $E_{g,P} = E_P$  is the bandgap of the topmost subcell and  $T_S$  is the temperature of the Sun. Eq. (10) is a generalization of  $V_{opt}$  found in the SJ literature. The expression reduces to the well-known SJ formula<sup>2,21,22</sup> for  $N=1$  with  $\langle E_g \rangle = E_{g,P}$ , as expected. A tool implementing this modeling framework is available online.<sup>23</sup>

Let us first consider a special case when  $Q=0$  (i.e., the bottom cell has the smallest bandgap), to illustrate the power of the technique. For arbitrary  $P$  and  $R$ , we have  $[Z] \equiv -[1, 0, \dots, \beta(1+R)X_0 - R]$ . Eq. (5) is now easily solved

$$X_i = \left( \frac{i}{\beta N} \right) + \frac{(N-i)[\beta(1+R)X_0 - R]}{\beta N}, \quad (11)$$

where  $i=1, \dots, N-1$ . With  $R=0$ , the equation reduces to the conventional tandem structure. As explained earlier,  $X_i$  is required to be mapped back to the “actual bandgap”  $E_i$ .

Interestingly, Eq. (11) offers a number of insights regarding the optimization of B-MJT cells. *First*, B-MJTs have smaller  $X_i$  than classical MJTs (i.e.,  $\Delta X_i = -(N-i)(1 - \beta X_0)R/\beta N$ ), because, given the albedo illumination, the bottom cells need not depend exclusively on the filtered light from the top; therefore, improved current matching is possible

even with reduced bandgap difference. *Second*, unlike standard MJT cells ( $R=0$ ), the bottom cell of an optimized B-MJT (with  $R>0$ ) need not have the smallest bandgap. Specifically, the condition that the bottom cell has the smallest bandgap implies  $X_1 - X_0 \geq 0$  for stacks with  $Q=0$ . Inserting the expression for  $X_1$  from Eq. (11) (derived for  $Q=0$ ) into this condition, we find

$$[(N-1)R - 1](\beta X_0 - 1) \geq 0.$$

For AM1.5G  $\beta = 0.428 \text{ eV}^{-1}$ , and Eq. (13) will show that  $X_0^{opt} \leq E_{SJ} (= 1.33)$  for an optimized B-MJT; therefore,  $(\beta X_0^{opt} - 1) < 0$ . Thus, an optimized tandem design (with  $Q=0$ ) is simply characterized by the constraint

$$N \leq (1 + R^{-1}). \quad (12)$$

For the  $(N, R)$  combination satisfying Eq. (12), the bottom cell has the smallest bandgap (i.e.,  $Q=0$ ), and thus we can use Eq. (11) to calculate the B-MJT cell design. This includes all conventional tandem cells because with  $R=0$ , Eq. (12) holds for arbitrary  $N$ . The condition also holds for a subset of B-MJT cells, with shorter stacks. For example, for symmetric illumination from top and bottom faces ( $R=1$ ), Eq. (12) is satisfied only for  $N \leq 2$ . The result is easily interpreted: With  $R=1$  and  $N > 2$ , symmetric illumination dictates that that B-MJT cells have a symmetric bandgap sequence, decreasing from the top to the middle, and then increasing again towards the bottom, so that  $Q=0$  is satisfied only with  $N \leq 2$ .



Focusing on the specialized case that satisfies Eqs. (11) and (12), we note that  $X_i$  depends on  $X_0$ , the smallest bandgap. Therefore, the B-MJTs must be optimized for  $X_0$  (or  $E_0$ ) for the maximum power output, as follows.

We first calculate numerically  $P_{\max} = J(V_{\text{opt}})V_{\text{opt}}$ , based on Equations (7), (9), and (10), to find  $\eta_T^*(E_0, N, Q = 0, R)$  for  $N = 1, \dots, 10$  and  $R = 0$ , and plot the results in Fig. 2(a). For comparison,  $\eta_T^*$  is the output normalized to the 1-sun input. The white squares mark the optimum  $E_0^{\text{opt}}(N)$  that maximizes  $\eta_T^*$  for a specified number of junctions. Figs. 2(b) and 2(c) show that the  $E_i$  associated with  $E_0^{\text{opt}}$  is in near perfect agreement with results reported in the literature for the classical ( $R = 0$ ) and bifacial cells ( $R = 0.3$ ), respectively. In Fig. 2(c) for  $R = 0.3$ , Eq. (11) can be used to find the bandgaps for  $N \leq (1 + R^{-1}) \sim 4$ —the results for  $N > 4$  must be optimized for  $Q > 0$ , see below. Given this level of agreement of the bandgaps shown in Fig. 2, it is not surprising that  $\eta_T^*$  matches with those from the literature as well, see Fig. 3.

In the discussion above, we have obtained the optimum- $E_0(N, R)$  for  $Q = 0$  through numerical maximization of the power-output. Fortunately, the result can also be estimated analytically, as follows. For a SJ ( $N = 1$ ) solar cell, the optimum bandgap is  $X_0 = X_{SJ} (\approx E_{SJ})$ . Due to the linearity of the  $J_{SC} - X_g$  relationship, the bandgaps  $\{X_i\}$  of the  $N$ -junction tandem would be such that the average is  $\langle X_i \rangle \approx X_{SJ}$ . (Note:  $\langle X_i \rangle = (X_0 + \dots + X_{N-1})/N$ ). Now, using this relation at the optimal with Eq. (11), we find

$$X_0^{\text{opt}} = \left( E_{SJ} - \frac{(N-1)(1-R)}{2\beta N} \right) \frac{2N}{N(1+R) + (1-R)}. \quad (13)$$

Here,  $E_{SJ} = 1.33 \text{ eV}$  is the SJ optimum bandgap. For AM1.5G, we have found  $X_0^{\text{opt}}$  to be within 0.5 to 1.5 eV—therefore, we can directly predict  $E_0^{\text{opt}} (= X_0^{\text{opt}})$  without mapping. Equation (13) anticipates the asymptotic limit of  $E_0^{\text{opt}}(N \rightarrow \infty)$  (see Figs. 2(b) and 2(c)), i.e.,

$$E_0^{\text{opt}}(N \rightarrow \infty) \approx \left( E_{SJ} - \frac{(1-R)}{2\beta} \right) \frac{2}{(1-R)}. \quad (14)$$

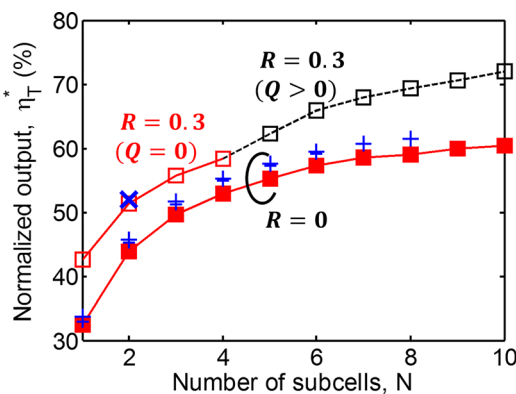


FIG. 3. The normalized output  $\eta_T^*$  for the B-MJT is shown for  $R = 0$  and  $R = 0.3$  by filled and open squares. Results are compared to theoretical predictions in the literature: for conventional tandem (+),<sup>13,14</sup> and bifacial tandem (×).<sup>10</sup> The black open squares (dashed lines) represent  $\eta_T^*$  for the optimized B-MJT at  $R = 0.3$  with  $Q \geq 0$ . Performance of the relevant state-of-the-art PV technologies can be found in Refs. 24–26.

The analytical results discussed thus far apply only to “ $Q = 0$ ” cells that satisfy Eq. (12). For  $Q > 0$ , we must optimize the stack numerically for arbitrary  $(N, R)$  combinations, as follows.

In general, for a given set of  $N, R, Q$ , and  $E_0$ , we first find the subcells bandgaps using Eq. (5) and by inverse mapping from  $X_g$  to  $E_g$  (also see Fig. S1 of supplementary material), and then calculate  $\eta_T^*(E_0, N, Q, R)$  using Equations (7), (9), and (10). For a given  $(N, R)$ , the maximum  $\eta_T^*$  determines  $E_0$  and  $Q$  simultaneously. The bandgap set for the globally optimized B-MJT at  $R = 0.3$  is shown in Fig. 2(c). For a bifacial tandem, the bottom subcells receive extra photons from the albedo. Therefore, for current matching and optimal designs: (i) the top subcells can be smaller to absorb more photons from the direct light and (ii) the bottom subcells can be larger to absorb fewer photons from the direct light as these subcells are compensated by the albedo. This results in a more tightly spaced set of bandgaps for B-MJTs (in Fig. 2(c)) compared to the conventional MJTs (in Fig. 2(b)). For  $R = 0.3$ , we observe that  $Q = 0$  for  $N \leq 4$ , consistent with the constraint in Eq. (12). For  $N > 4$ ,  $\eta_T^*$  is maximized for  $Q > 0$ , that is, the cell with the smallest bandgap is no longer located at the bottom. This allows the bottom cell to fully benefit from the albedo light. The  $Q$ -values are marked at the top-axis in Figs. 2(c).

The corresponding output  $\eta_T^*$  for the optimized cells discussed above is marked in Fig. 3. One may naively expect that when the sunlight intensity is scaled by a factor of  $(1 + R) = 1.3$ , the output will increase by a factor of  $(1 + R) = 1.3$  as well. The requirement of current matching among the series connected subcells, however, restricts the ultimate gain below the idealized limit. Indeed for  $N = 1$ , the efficiency increases from  $\sim 31\%$  at  $R = 0$  to  $\sim 40.3\%$  at  $R = 0.3$ , a 30% gain as expected. The gain is somewhat smaller for  $N > 1$  due to the constraint of current matching in B-MJTs.

While the results for  $R = 0$  (classical tandem) are only of pedagogical interest, the results shown in Fig. 3 report the efficiency gain of B-MJTs with  $N \geq 3$ , which have not been discussed in the prior literature. The results suggest that a 4-junction B-MJT (at a practical  $R = 0.3$ ) would outperform a 7-junction classical MJT, such as the power of the current-constraint relaxed by the bifacial concept. For the same  $N$ , the increased power-input of B-MJT would make the cells slightly hotter, but the reduced temperature coefficient of some of the bifacial cells, such as HIT (Hetero-junction with Intrinsic Thin-layer), would compensate the effect.

To conclude, we have developed a methodology that can be used to answer a broad range of questions regarding conventional as well as bifacial tandem cells. The series connected circuit approach allowed us to derive expressions for  $J_{\text{dark}}$  and  $V_{\text{opt}}$ . We have generalized the physically meaningful expression for  $V_{\text{opt}}$ , which is valid for SJs, MJTs, and B-MJTs. Our analysis presents analytical expressions estimating the bandgap sequence for conventional MJTs and B-MJTs (for  $N \leq (1 + R^{-1})$ ). Numerical simulations would still be necessary for MJTs or B-MJTs involving extremely large or small bandgaps, or for optimization at the maximum power point involving luminescent coupling.<sup>19,20</sup> The final

design must rely on careful numerical optimization of finite absorption, reflection, and series resistance. Regardless, the methodology reported here stands out in its simplicity and versatility to quantitatively predict a range of phenomena previously accessible only to numerical modeling.

See [supplementary material](#) for  $J_{SC}$  vs. bandgap plot in Fig. S1, circuit model for tandems in Fig. S2, and detailed results for B-MJT in Figs. S3–S6, derivation for constraint on  $N$  for  $Q = 0$ .

We acknowledge Professor J. L. Gray, Professor Mark Lundstrom, and Professor P. Bermel for helpful discussions. This work was supported by the DOE-SERIIUS and NSF-NEEDS centers. We gratefully acknowledge research support from the NCN NEEDS program, which is funded by the NSF (Contract 1227020-EEC), and the Semiconductor Research Corporation. This work was also supported by the Solar Energy Research Institute for India and the United States (SERIIUS), funded by the US Department of Energy under Subcontract DE-AC36-08GO28308 and the Government of India, through the Department of Science & Technology under Subcontract IUSSTF/JCERDC-SERIIUS/2012.

<sup>1</sup>W. Shockley and H. J. Queisser, “Detailed balance limit of efficiency of p-n Junction solar cells,” *J. App. Phys.* **32**, 510 (1961).

<sup>2</sup>L. C. Hirst and N. J. Ekins-Daukes, “Fundamental losses in solar cells,” *Prog. Photovolt: Res. Appl.* **19**, 286–293 (2011).

<sup>3</sup>S. Dongaonkar, C. Deline, and M. Alam, “Performance and reliability implications of two-dimensional shading in monolithic thin-film photovoltaic modules,” *IEEE Journal of Photovoltaics* **3**, 1367–1375 (2013).

<sup>4</sup>T. Silverman, M. Deceglie, X. Sun, R. Garris, M. Alam, C. Deline, and S. Kurtz, “Thermal and electrical effects of partial shade in monolithic thin-film photovoltaic modules,” *IEEE Journal of Photovoltaics* **5**, 1742–1747 (2015).

<sup>5</sup>*Handbook of Photovoltaic Science and Engineering*, 2nd ed. edited by A. Luque and S. Hegedus (John Wiley & Sons, Ltd., 2011).

<sup>6</sup>C. H. Henry, “Limiting efficiencies of ideal single and multiple energy gap terrestrial solar cells,” *J. Appl. Phys.* **51**, 4494–4500 (1980).

<sup>7</sup>U. Yusufoglu, T. Pletzer, L. Koduvelikulathu, C. Comparotto, R. Kopecek, and H. Kurz, “Analysis of the annual performance of bifacial modules and optimization methods,” *IEEE Journal of Photovoltaics* **5**, 320–328 (2015).

<sup>8</sup>A. Luque, E. Lorenzo, G. Sala, and S. López-Romero, “Diffusing reflectors for bifacial photovoltaic panels,” *Solar Cells* **13**, 277–292 (1985).

<sup>9</sup>R. Asadpour, R. V. K. Chavali, M. R. Khan, and M. A. Alam, “Bifacial Si heterojunction-perovskite organic-inorganic tandem to produce highly efficient ( $\mu T^*$  33%) solar cell,” *Appl. Phys. Lett.* **106**, 243902 (2015).

<sup>10</sup>M. R. Khan and M. A. Alam, “Thermodynamic limit of bifacial double-junction tandem solar cells,” *Appl. Phys. Lett.* **107**, 223502 (2015).

<sup>11</sup>A. D. Vos, “Detailed balance limit of the efficiency of tandem solar cells,” *J. Phys. D: Appl. Phys.* **13**, 839 (1980).

<sup>12</sup>A. Martí and G. L. Araújo, “Limiting efficiencies for photovoltaic energy conversion in multigap systems,” *Solar Energy Materials and Solar Cells* **43**, 203–222 (1996).

<sup>13</sup>S. P. Bremner, M. Y. Levy, and C. B. Honsberg, “Analysis of tandem solar cell efficiencies under AM1.5G spectrum using a rapid flux calculation method,” *Prog. Photovolt: Res. Appl.* **16**, 225–233 (2008).

<sup>14</sup>A. S. Brown and M. A. Green, “Detailed balance limit for the series constrained two terminal tandem solar cell,” *Physica E: Low-dimensional Systems and Nanostructures* **14**, 96–100 (2002).

<sup>15</sup>A. Luque, A. Cuevas, and J. Ruiz, “Double-sided n+-p-n+ solar cell for bifacial concentration,” *Solar Cells* **2**, 151–166 (1980).

<sup>16</sup>A. Cuevas, A. Luque, J. Eguren, and J. del Alamo, “50 Per cent more output power from an albedo-collecting flat panel using bifacial solar cells,” *Solar Energy* **29**, 419–420 (1982).

<sup>17</sup>H. Ohtsuka, M. Sakamoto, K. Tsutsui, and Y. Yazawa, “Bifacial silicon solar cells with 213% front efficiency and 198% rear efficiency,” *Prog. Photovolt: Res. Appl.* **8**, 385–390 (2000).

<sup>18</sup>M. Alam and R. Smith, “A phenomenological theory of correlated multiple soft-breakdown events in ultra-thin gate dielectrics,” in *41st Annual 2003 IEEE International Symposium Proceedings on Reliability Physics* (2003), pp. 406–411.

<sup>19</sup>M. A. Steiner and J. F. Geisz, “Non-linear luminescent coupling in series-connected multijunction solar cells,” *Appl. Phys. Lett.* **100**, 251106 (2012).

<sup>20</sup>D. Lan, J. F. Geisz, M. A. Steiner, I. Garcia, D. J. Friedman, and M. A. Green, “Improved modeling of photoluminescent and electroluminescent coupling in multijunction solar cells,” *Solar Energy Materials and Solar Cells* **143**, 48–51 (2015).

<sup>21</sup>P. T. Landsberg and V. Badescu, “Carnot factor in solar cell efficiencies,” *J. Phys. D: Appl. Phys.* **33**, 3004 (2000).

<sup>22</sup>M. A. Alam and M. R. Khan, “Fundamentals of PV efficiency interpreted by a two-level model,” *American Journal of Physics* **81**, 655–662 (2013).

<sup>23</sup>M. R. Khan, X. Jin, and M. A. Alam, “PVLimits: PV thermodynamic limit calculator,” 2016, see <https://nanohub.org/resources/pvlimits>.

<sup>24</sup>M. A. Green, K. Emery, Y. Hishikawa, W. Warta, and E. D. Dunlop, “Solar cell efficiency tables (version 45),” *Prog. Photovolt: Res. Appl.* **23**, 1–9 (2015).

<sup>25</sup>M. A. Green, K. Emery, Y. Hishikawa, W. Warta, and E. D. Dunlop, “Solar cell efficiency tables (version 46),” *Prog. Photovolt: Res. Appl.* **23**, 805–812 (2015).

<sup>26</sup>M. A. Green, K. Emery, Y. Hishikawa, W. Warta, and E. D. Dunlop, “Solar cell efficiency tables (version 47),” *Prog. Photovolt: Res. Appl.* **24**, 3–11 (2016).